

Characterization of the Interaction between Cationic Thulium (III) – Porphyrin Complex with Bovine Serum Albumin

Xi-Liang Lu^{1,2*}, Huai-Cheng Yang², Hui Wu³ and An-Xin Hou¹

¹College of Chemistry and Molecular Sciences, Wuhan University, Wuhan 430072, PR China

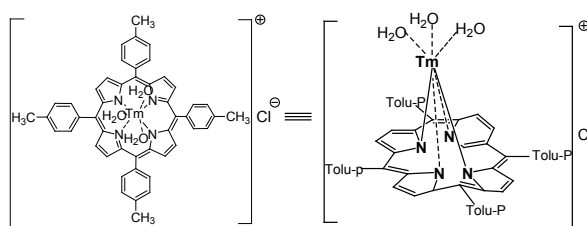
²Department of Chemistry, Guilin Normal College, Guilin GuangXi 541002, PR China

³Department of Chemistry, Wuhan University of Technology, Wuhan 430070, PR China

Abstract

The interaction of cationic Thulium (III)–porphyrin complex (Tm–Porp) with Bovine Serum Albumin (BSA) has been investigated by fluorescence quenching spectra. The quenching mechanism of fluorescence was suggested as a static quenching with a high-affinity according to the Stern–Volmer equation. The number of binding sites and the apparent binding constant K_a of the Tm–Porp on BSA were explained by a modified Scatchard equation and the site probe competition. The corresponding thermodynamic parameters ΔH^0 , ΔG^0 and ΔS^0 at different temperatures are discussed. The results indicated that the electrostatic and hydrophobic interactions are the predominant intermolecular forces in stabilizing complex. Binding distance between the donor and acceptor was obtained in terms of Forester's Non-radiative energy transfer theory. Furthermore, the effects of the Tm–Porp on the BSA configuration were elucidated by Circular Dichroism (CD) spectra method along with UV–Vis absorption and Synchronous Fluorescence Spectroscopy (SFS). The results indicated that the secondary structures of BSA have been perturbed in the presence of drug. Finally, we showed that the cationic Tm–Porp can preferentially bind at the site-I and site-II of BSA with equal occupancy.

Graphical abstract: The binding of Tm–Porp with BSA was investigated at different temperatures by fluorescence, UV–Vis absorption spectrum, CD spectrum and SFS at pH 7.40.



Keywords: Cationic Thulium(III)–Porphyrin (Tm–Porp); Bovine serum albumin (BSA); Fluorescence quenching ; Non-radiative energy transfer; Circular dichroism (CD); Synchronous fluorescence spectroscopy (SFS)

Introduction

There has been a growing interest in the application of porphyrins and its related compounds as therapeutic drugs for the last decade [1–4]. Metalloporphyrins, especially the rare earth metal porphyrins and its complexes have been utilized extensively in the direction of diagnostic of diseases and therapeutic agents. Potential applications of these have appeared in the treatment of non-malignant conditions such as viral and bacterial infections, including the human immunodeficiency virus (HIV) [5], and great many of the important results were continuously be acquired [6–7]. The study found that some rare earth metals possess a special affinity to be tumor cells, for example, the 70% of ¹⁶⁹Yb accumulated in tumors 10 minutes after intravenous injection. These carrier molecules can interact preferentially or specifically with cancer cells and accumulate in malignant tumor. The first monoporphyrate lanthanide (III) complex was reported early in 1974 [8] and since then only a few studies on these systems have previously appeared in the literature. Thulium was among those considered as the most suitable element for the detection of tumors, in respect that it has the highest affinity for serum albumin in particular for its binding site II [9]. Moreover, some synthetic porphyrins and metalloporphyrins have been applied to detect of early-stage tumors and work in the field of Photodynamic Therapy (PDT) on tumors [7,10]. Nevertheless, drug delivery of porphyrins to tumor cells was the major challenge in the detection, and this has been achieved partly by using selective delivery

systems such as monoclonal antibodies, liposomes, and albumins [1]. A typical compound: meso-Tetrakis (3-hydroxyphenyl) porphyrin is a powerful photosensitizer for PDT when accumulate preferentially in tumor tissue in comparison with normal muscle tissue. And it is now undergoing clinical trials [11]. However, most research concerning antibacterial compounds of metalloporphyrins have been localized on several of lanthanide cationic, such as Ln (III), Yb (III), Pr (III), and Tm (III) and have focused merely on the interaction with DNA or microorganisms [12–13]. Another example is the fact that heavy metal arsenic had affinity for site II of BSA [14], the presence of arsenic and drug with high affinity for site II of BSA will have changes the pharmacokinetics of these drugs during concurrent administration of drug and arsenic. If so, we need to take into account the prescribing of those drugs to avoid the arsenic affecting human life and health. Thus, studies on specific serum albumin binding may be highly pertinent as a model for mitochondrial interactions with metalloporphyrins. This suggests that we ought to pay extensive attention to their biological

***Corresponding author:** Xi-Liang Lu, Department of Chemistry, Guilin Normal College, Guilin GuangXi 541002, PR China, Tel: +86-773-2148-118; E-mail: ludidi@126.com

Received October 2010, 2012; Accepted April 05, 2012; Published April 09, 2012

Citation: Lu XL, Yang HC, Wu H, Hou AX (2012) Characterization of the Interaction between Cationic Thulium (III)–Porphyrin Complex with Bovine Serum Albumin. J Mol Biomark Diagn 2:126. doi:10.4172/2155-9929.1000126

Copyright: © 2012 Lu XL, et al. This is an open-access article distributed under the terms of the Creative Commons Attribution License, which permits unrestricted use, distribution, and reproduction in any medium, provided the original author and source are credited

activity, pharmacological effects and pharmacokinetics in vivo. In this work, we aim to investigate the interaction of the lanthanide-porphyrin complex [Tm (TTP) (H₂O)₃] Cl (Tm–Porp, Figure 1), (TTP=5,10,15,20-tetrakis (4-tolyl) porphyrinate dianion) with BSA by fluorescence quenching spectroscopy and SFS in comparison to other lanthanide-porphyrin ligands. The affinity of Tm–Porp binding on protein has been characterized by quenching method. We also examined the effect of the drug on the conformational changes of BSA based on the UV-Vis absorption, CD and SFS.

Experimental

Materials

BSA was purchased from Sigma Chemical Co., Ltd. Tm–Porp was prepared by the classical method of Alder [15] and characterized by the literature [12]. Tris–Base (2-amino-2-(hydroxymethyl) -1, 3-propanediol) had a purity of not less than 99.5%, and NaCl, NaOH and HCl, etc., were all of analytical purity. Protein was dissolved in Tris–HCl buffer solution (0.05 mol l⁻¹ Tris, 0.15 mol l⁻¹ NaCl, pH 7.40) to form an identical concentration of 1 mM stock solution. The concentration of the protein was determined spectrophotometrically using an extinction coefficient ($\epsilon=280$) of 44000 M⁻¹cm⁻¹. Amaranthine crystallographic cationic Tm–Porp was prepared by absolute Dimethylformamide (DMF) to form 1 mM as the stock solution. (Molecular weight=925.3 g/mol) and its final concentration in titration was equal to BSA's. Warfarin sodium was supplied by Medicine Co., Ltd., Jiangsu (China) and Ibuprofen (99.7%) was purchased from Wuhan Galaxy Chemical Co., Ltd., both prepared by absolute DMF to form 1 mM solution. For CD spectroscopy, the cationic Tm–Porp used in our experiments is not optically active, and thus it alone did not show any CD signal. BAS and drug were dissolved in the sodium phosphate buffer (PBS, 10 mM, pH 7.40) to be prepared as a 1 mM stock solution and both stored in an icebox at 0–4°C. All other reagents were of analysis- grade chemicals. Triply distilled and deionized water was used throughout and a fresh stock solution of proteins would be applied to all experiments.

Fluorescence and UV–Vis absorbance spectroscopy

The fluorescence quenching measurements were carried out by a RF-2500 model spectrofluorometer (Shimadzu, Japan), which equipped with a Xenon lamp and a thermostat bath. FL WinLab recording spectrophotometer (Perkin-Elmer, Inc., USA) equipped with a 1.0 cm-path length quartz cuvette and a self-acting thermostat were held in the scan all spectrum-related regions. The slit width for the excitation and emission monochromator was 5 nm. The fluorescence emission spectra, following 280 nm excitation, were collected at 3 temperatures (297,304 and 310 K) in the range of 300–550 nm. In order to assess the effect of self-absorption of Tm–Porp on its emission spectrum, we

are required to determine a shift effect with 3 different concentrations of drug (10⁻³, 10⁻⁴ and 10⁻⁵ M) at 297 K. The results obtained (data not shown) displayed that the emission spectra shift dramatically to longer wavelengths at a higher concentration (10⁻³ M) but it is inconspicuous at a lower concentration (10⁻⁵ M) when spectra of DMF were always subtracted from the experimental data to correct for background. Consequently, we did not take this effect of drug into account in the range of 270–300 nm. Inner filtration was negligible because of the fluorescence measured intensity (the emission band at 350 nm) is proportional to optical intensity of drug at 280 nm (by using a 1×1 cm quartz cuvet constantly) is less than 0.05 when the absorbance of drug solution at excitation and emission wavelengths was provided with Aex (=0.4) and Aem (=0.5), respectively [16]. We have also neglected the scattering effects on emission spectra because of the high ratio between absorption and light scattering cross-sections [17]. Dilute solutions were prepared in the investigated region (BSA 10 μM, Tm–Porp in the range of 0–100 μM) to avoid inner filter effect. We have collected the quenching spectra by using a microinjector with a sequential injection of the various volumes of a 10 μM Tm–Porp solution at 3 recorded temperatures, and each quenching spectra were registered in triplicate with virtually identical results.

The synchronous fluorescence spectra (Luminescence Spectrometer LS-55, Perkin Elmer, USA) were performed under the following conditions: the emission wavelength was collected at room temperature in the range 200–500 nm. The initial excitation spectral range was 200–350 nm with increment of 5 nm by using excitation / emission=10/4.0 nm slit widths, equipped with 700V PMT (photo multiplier tube). The range of synchronous scanning was $\lambda_{ex}=250$ –275 nm, $\lambda_{em}=310$ –290 nm, where the differences in the wavelengths ($\Delta \lambda$) were 60 nm ($\lambda_{ex}=250$ nm, $\lambda_{em}=310$ nm) and 15 nm ($\lambda_{ex}=275$ nm, $\lambda_{em}=290$ nm). The other optimum scanning parameters were introduced just the same as those of the fluorescence quenching spectra mentioned above.

Absorbance spectra were collected using distilled water (the electrical conductivity was less than 0.10 mS/m at 297 K) as the reference by a double beam TU-1901 UV–Vis spectrophotometer (Puxi Analytic Instrument Ltd. of Beijing, China), and absorption cell was a 2–ml with a 1–cm path length quartz cuvette. The investigated spectral range was 220–400 nm with a 2-nm bandwidth. To bring absorbance spectra to pass, a 2.0 mL solution of 10 μM BSA was titrated by sequential addition of the drug solution and by using trace syringe to scan a spectral curve versus a blank of buffer.

Circular dichroism measurements

CD spectra were recorded at the ambient temperature by a Jasco J-810 spectropolarimeter (Tokyo, Japan), which had a 1.0 mm pathlength of optical circular quartz cells at 1 nm length data pitch intervals. The investigated spectral range was 190–260 nm with accumulation 3 scans averaged for each spectrum by using a scan data pitch of 0.1 nm. Scan slit width of 1 nm and scan rate of 500 nm/min were constantly taking place. We mixed drug into a 2.0 mL solution of 5.0 μM BSA in a plastic cuvette then allowed to react for 10 minutes in the PBS buffer solution for gaining the difference spectrum. Each cuvette containing Tm–Porp was obtained in the concentration range 0 to 0.30 mmol/L after transfer into a quartz cell. The CD spectra of BSA in the absence and presence of drug had a molar ratio of concentration Tm–Porp to BSA (R) ranging from 0.0 to 3.0 under constant nitrogen flush. The α -helical was expressed in terms of Mean Residue Ellipticity (MRE) by using the mean residue weights of 113.2 (66000/583) for the

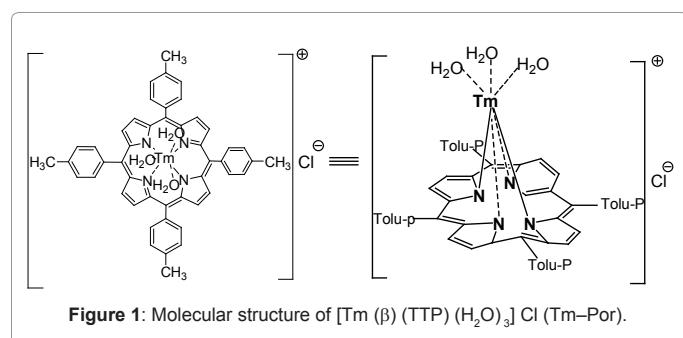


Figure 1: Molecular structure of [Tm (β) (TTP) (H₂O)₃] Cl (Tm–Porp).

intact molecule of BSA, the CD spectrum of buffer solution as reference was subtracted from the sample spectra to correct for background.

Results and Discussion

Fluorescence quenching mechanism and binding parameters

Fluorescence quenching can be dynamic, resulting from collisional encounters between the fluorophore and quencher, or static, resulting from the formation of a ground state complex between fluorophore and the quencher [18]. Static and dynamic quenching can be distinguished by their different binding constants: dependence on temperature and viscosity, or preferably by lifetime measurements.

Figure 2 shows the effect of increasing the concentration of Tm-Porp on the fluorescence emission spectra of BSA. With a stepwise increasing concentration of Tm-Porp, it seems that where the BSA's fluorescent intensity at around 342 nm was quenched attended by selectively decreased of the emission band at excitation wavelength 280 nm. We suggest that this phenomenon could refer to a high affinity-binding site on an adjacency tryptophan (Trp) and/or tyrosine (Tyr) of protein. Since Tm-Porp had no intrinsic fluorescence in this range, the microenvironment around chromophore of BSA was changed after adding Tm-Porp with no distinct red shift in emission wavelength. It thus can be deduced that the interaction has occurred and the energy has been transferred.

It is assumed that this procedure was discussed to be a dynamic fluorescence quenching, which can be described by Stern-Volmer equation:

$$F_0 / F = 1 + k_q \tau_0 [Q] = 1 + K_{SV} [Q] \quad (1)$$

Where k_q , K_{SV} , τ_0 and $[Q]$ are the quenching rate constant of the biomolecular [$M^{-1}s^{-1}$], the dynamic Stern-Volmer quenching constant [M^{-1}], the average lifetime of BSA and the concentration of quencher [M], respectively. F_0 and F are the fluorescence intensities in the absence and presence of quencher, respectively. In respect that fluorescence lifetime of biopolymers τ_0 is 10^{-8} s [19], quenching constant k_q at pH 7.40 can be obtained by means of linear fitting method. The Stern-Volmer plot (Figure 2) of F_0 / F against $[Q]$ from Equation.(1) at different temperatures can also be collected through experimental data. The values of k_q Correspondingly are: 297 K, $1.35 \times 10^{13} M^{-1}s^{-1}$, 304 K, $1.12 \times 10^{13} M^{-1}s^{-1}$ and 310 K, $1.01 \times 10^{13} M^{-1}s^{-1}$, respectively. However, the maximum scatter collision quenching constant, k_q , of various kinds of quenchers with biopolymers is $2.0 \times 10^{10} M^{-1}s^{-1}$ [19]. The rate constant of protein quenching procedure initiated by drug is obviously greater than k_q of scatter procedure, which indicates that the quenching of BSA by Tm-Porp is not initiated by dynamic collision but involved in forming complexes with a static procedure. And the values of K_{SV} decreased with the rising of the temperature (see Table 1), this may be the result of non-radiative energy transfer between the drug and BSA. So dynamic collision could be negligible in quantitative analysis [20].

For a more detailed exploration of the molecular mechanism of protein-drug interaction and their structural changes, we further investigate the effect of UV-Vis absorption spectra of the Tm-Porp-BSA complex (Figure 3). The region where a main changes can be observed is the maximum peak height (in the range 200-280 nm) of BSA to go with a red shift from 233 nm to 239 nm when BSA combined with the drug, implying that there is the formation of a ground state complex between chromophore and drug [17]. Thus the mechanism of fluorescence quenching was a static quenching and the binding constant (K_a) with the thermodynamic parameters can be evaluated by the thermodynamic method in the data analysis.

In the case of an ambient temperature experiment, the reaction enthalpy change is regarded as a constant. According to both Van't Hoff equation and chemical thermodynamical functions, for the binding constant and thermodynamic parameters are given by

$$\ln K_a = -\Delta H^\circ / RT + \Delta S^\circ / R \quad (2)$$

$$\Delta G^\circ = -RT \ln K_a = \Delta H^\circ - T\Delta S^\circ \quad (3)$$

were ΔH° , ΔG° and ΔS° are enthalpy change, Gibbs free energy change and entropy change, respectively. The values of these parameters

PH	T (K)	linear Fitting	$K_{SV} [M^{-1}]$	$Kq (M^{-1}s^{-1})$	R	S.D.
7.40	297	$F_0/F=0.6504+1.352 \times 10^{13}[Q]$	1.35×10^5	1.35×10^{13}	0.9973	0.064
7.40	304	$F_0/F=0.8795+1.117 \times 10^5 [Q]$	1.12×10^5	1.12×10^{13}	0.9988	0.023
7.40	310	$F_0/F=0.8683+1.018 \times 10^5 [Q]$	1.02×10^5	1.02×10^{13}	0.9936	0.048

R: linear correlated coefficient; S.D.: standard deviation

Table 1: Stern–Volmer quenching constant (K_{SV}) of the interaction of Tm-Porp with BSA measured by fluorimetric titrations.

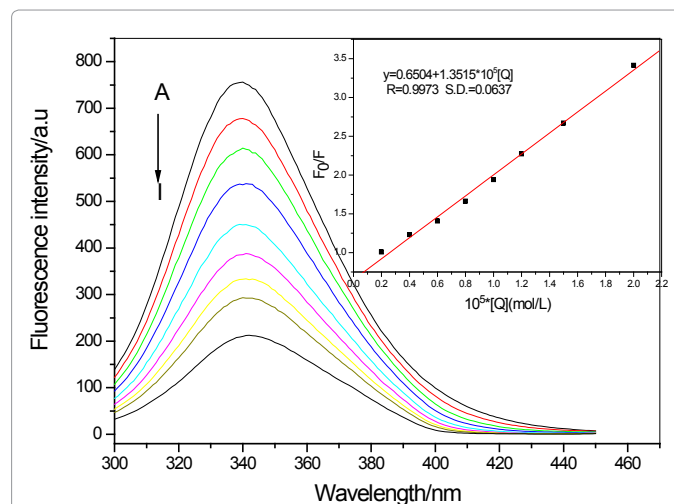


Figure 2: fluorescence spectra of BSA in the presence of Tm-Por. at pH=7.40, 297K, $\lambda_{Ex}=280$ nm. $c(\text{BSA})=10 \mu\text{M}$; $c(\text{Tm-Por})/(10 \mu\text{M})$, A \rightarrow 1:0, 0.2, 0.4, 0.6, 0.8, 1.0, 1.2, 1.5, 2.0. Inset: the relationship of F_0/F and the concentration of quenching agent Tm-Por.

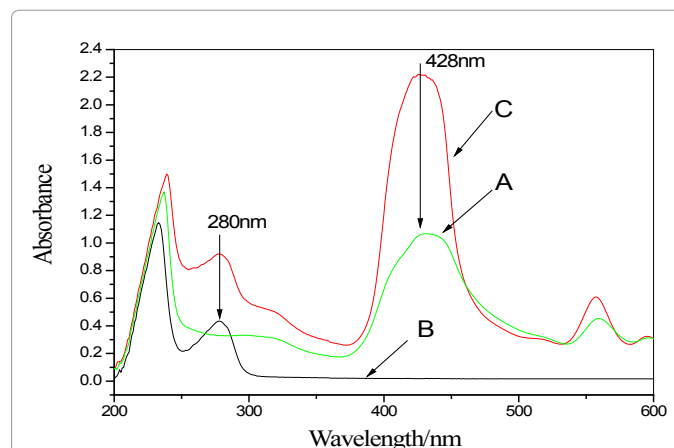
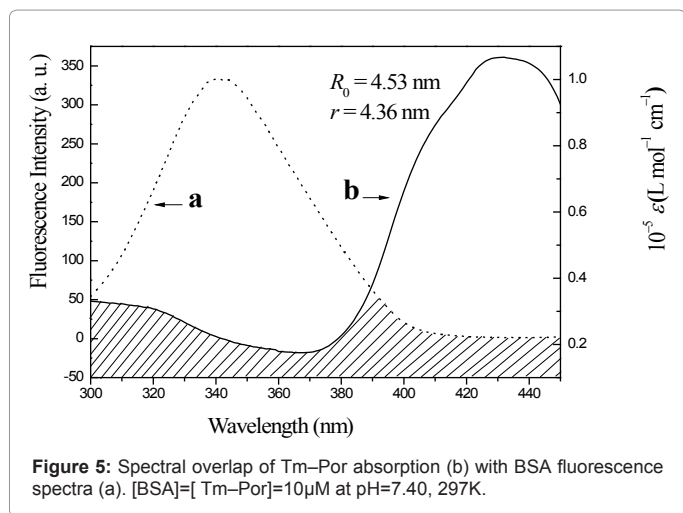
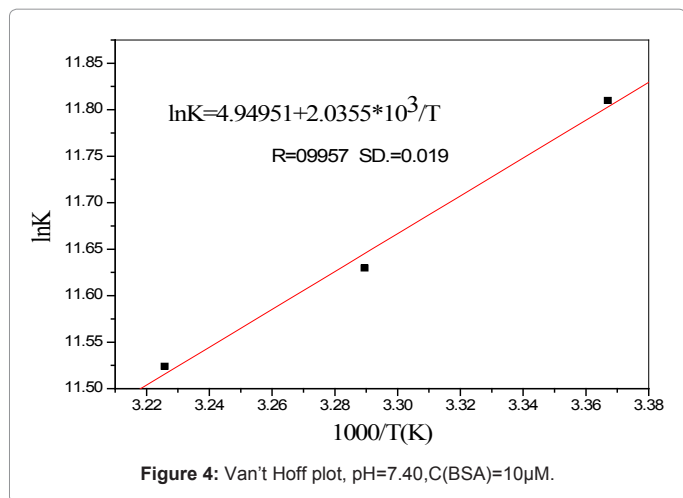


Figure 3: The UV-vis absorption spectra of BSA and BSA– Tm-Porp system. (A) The absorption spectrum of Tm-Porp only; (B) The absorption spectrum of BSA only; (C) The absorption spectra of BSA–Tm-Porp at the same concentration; $c(\text{BSA}) = c(\text{Tm-Porp}) = 10 \mu\text{M}$ at pH=7.40, 297K.



can be simultaneously acquired by using a least-squares algorithm for data-fitting (viz., a linear of $\ln K_a$ versus $1/T$ of Van't Hoff plot, T is the absolute temperature and K_a is the apparent binding constant) according to Eqs. (2) and (3) (Figure 4.). These consequences together with the correlated coefficient are listed in (Table 2). For $\Delta H^\circ < 0$, $\Delta S^\circ > 0$, positive entropy is frequently taken as evidence for hydrophobic interaction when a biomolecule interacts with protein according to Ross and Subramanian's rules [21]. Moreover, the negative ΔH° may be a manifestation of electrostatic interaction [22]. In fact, the cationic Tm-Por carries a positive charge in aqueous solution, which might be identified the electron-rich amino acid residues contributing to the binding of the drug molecules. Then, the relatively smaller positive entropy change and a little negative enthalpy change indicate that hydrophobic interaction force cannot be excluded. In particular, the gigantic hydrophobic cavity of the porphyrin ring of drug, wherein the accommodating fragments of Trp213 or Trp134, would then redound to the hydrophobicity of Trp more than those of unbound chromophores. The non polarity of Trp residues was strengthened by the amino acid residues of protein around the porphyrin ring, by a preferential orientation of electric attraction. Accordingly, the hydrophobic interaction should play a major role between BSA and the drug accompanied by the electrostatic force. Furthermore, the value of ΔG° and ΔH° indicates that the interaction process is spontaneous

and exothermic with a concomitant increase of entropy at a constant temperature of 24°C.

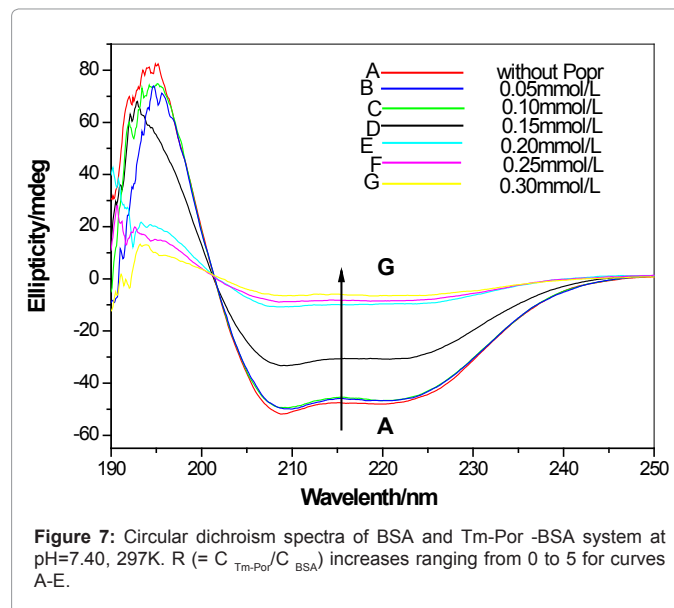
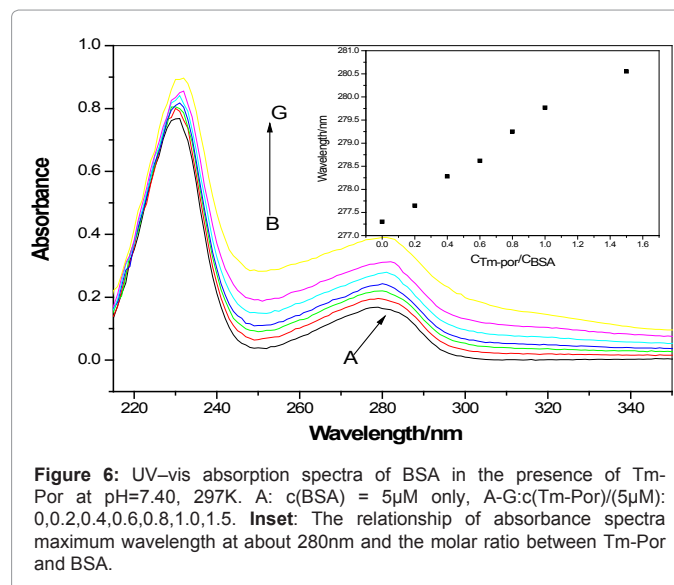
The number of binding sites and localization

If a drug binds with protein independently to only one set of equivalent sites and with no cooperative effects to form a static complex, we can introduce the equilibrium between free and bound molecules using a modified Scatchard relationship [23]:

T (K)	K_a (M^{-1})	ΔH° (KJ/mol)	ΔG° (J/mol)	ΔS° (KJ/mol)	R
297	5.57×10^5	-16.92	41.15	-29.14	0.9944
304	2.80×10^5	-16.92	41.15	-29.43	0.9981
310	1.05×10^5	-16.92	41.15	-29.68	0.9961

R: correlated coefficient

Table 2: The apparent binding constant K_a and relative thermodynamic parameters at pH 7.4.



$$\frac{F_0}{F} = -K_a n \cdot [P_i] + K_a [D_i] \cdot \frac{F_0}{F_0 - F} \quad (4)$$

where F_0 and F are the fluorescence intensity in the absence and presence of quencher (drug), K_a and n are the apparent binding constant and the number of (strong) binding sites, $[D_i]$ and $[P_i]$ are the final concentration of the drug and the protein, respectively. Thus, we can also obtain K_a as well as the number of binding site (n) of the drug with BSA from the intercept and slope of the linear dependence of F_0/F vs. $[D_i] \cdot [F_0/(F_0 - F)]$. The value of K_a was shown in (Table 2), and the value of n was 1.80 (297 K, 1.23(304 K) and 0.29 (310 K) at $c(\text{BSA}) = c(\text{Tm-Porp}) = 10 \mu\text{M}$, respectively. The results of the apparent binding constant (K_a) presented in table are greater than or equal to 10^5M^{-1} , which suggests that Tm-Porp selectively quenches the fluorescence emission intensity of protein via a high-affinity binding site. For the number of binding sites approximates to 2 at room temperature, we have been able to determine that the molecules of drug are distributed between two different binding sites. Incidentally, the number of binding sites has been caused a rapid diminution when the temperature rises to 310 K, which may be ascribed to perturbation of the weak affinity binding site-I of BSA and the movement of the fluorophore discussed below.

To further gain insight into the binding site of the drug on BSA, the competitive displacement experiment was performed in our lab. The main best-characterized drug binding sites are site-I or warfarin (WF) site (in subdomain IIA) and site-II (benzodiazepine site or Sudlow's drug site [24]), formed by a binding pocket in subdomain IIIA. Here we used a widely prescribed anticoagulant and the high-affinity WF as a site marker for competitive trial reagent. The typical benzodiazepine site ligands Ibuprofen (IBP) as a site marker were simultaneously taken for present purposes. The experiment was carried out at 297 K and also by utilizing Trp of BSA as an intrinsic fluorescence spectra probe at an excitation 280 nm for warfarin (WF:BSA=1:1, Tm-Porp=0~60 μM) and for diazepam (IBP:BSA=1:1, Tm-Porp=0~60 μM). Interestingly, the fluorescence intensity of both decreased regularly with increasing of Tm-Porp concentration, the values of quenching constant K_{sv} of BSA from 1.35×10^5 (unbound) dropped to $0.75 \times 10^5 \text{M}^{-1}$ (bound to WF), and the values of quenching constant K_{sv} of BSA also from $1.35 \times 10^5 \text{M}^{-1}$ (unbound) dropped to $0.77 \times 10^5 \text{M}^{-1}$ (bound to IBP). Therefore, as we expected, the effects of warfarin and ibuprofen would contribute to both spectral intensity enhancements, which were similar to BSA in the presence of the drug. The two probes have almost identical effects on the Stern-Volmer quenching constant, implying that the binding of BSA to Tm-Porp must have been simultaneously sharing two different binding sites with WF and IBP. The binding sites of Tm-Porp to BSA are non-specific one and no selectivity [25]. In this regard, there must be pairing sites, I and II (in subdomains of IIA and IIIA, respectively) that both were responsible for the interaction of protein with various ligands in two orientation dimensions with equal occupancy. Similar with WF binding upon HAS [26], Tm-Porp can provide moiety of O atoms (3 centrally coordinated H₂O molecules, Figure 1), which aggrandizes hydrophobic contacts and intensifies the apolar of the surroundings. For the existence of the intrinsic high-affinity interplay between the cationic Tm (III) center and electron-rich amino acid side chain residues of BSA, such as disulfides, histidine (His67, His247) and those metal ion sites [27], we can inferred that the predominant involvement of non-specific electrostatic interaction was promoting a preferential orientation angle and had a decrease in the distance between these two ends of two binding sites.

Furthermore, we can assess the quantity of spatial binding distance

between the drug and Trp213 (or Trp134) moieties of BSA according to Förster's non-radiative energy transfer theory [28]. The Fluorescence Resonance Energy Transfer (FRET) is not only depended on the spatial distance (r) between acceptor (Tm-Porp) and donor (the binding site-I and site-II of BSA), but also related to the critical energy transfer distance (R_0) as

$$E = 1 - \frac{F}{F_0} = \frac{R_0^6}{R_0^6 + r^6} \quad (5)$$

Where R_0 is the critical distance when the transfer efficiency comes up to 50%, and

$$R_0^6 = 8.8 \times 10^{-25} K^2 N^{-4} \cdot \Phi \cdot J \quad (6)$$

Thus, K^2 is the spatial-orientation factor of the dipole, N is the refractive index of the medium, Φ is the fluorescence quantum yield of the donor (Trps) and J is the overlap integral of the fluorescence emission spectrum of the donor and the absorption spectrum of the acceptor. Then overlap integral is defined as

$$J = \frac{\int_0^\infty F(\lambda) \varepsilon(\lambda) \lambda^4 d\lambda}{\int_0^\infty F(\lambda) d\lambda} \quad (7)$$

Where $F(\lambda)$ is the corrected fluorescence intensity of the donor in the wavelength range from λ to $\lambda + \Delta\lambda$ and $\varepsilon(\lambda)$ is the extinction coefficient of the acceptor at λ . By integrating the spectra, we could confirm the overlap between the absorption spectra of Tm-Porp and the fluorescence emission spectra of BSA-Tm-Porp in a wavelength range of 300-450 nm as shown in (Figure 5). In the present experimental conditions, $N=1.36$, $K^2=2/3$, $\Phi=0.15$ [29], so J and R_0 can be estimated from Eq. (7), Eq. (6) and Figure 5. [$J=3.36 \times 10^{-14} \text{cm}^3 \cdot \text{M}^{-1}$, $R_0=4.53 \text{nm}$]. And the spatial distance between Tm-Porp and the amino acid (Trp) residues of BSA is $r=4.36 \text{nm}$. Moreover, the efficiency of FRET is 56 % from Equation. (5).

The average spatial binding distance $r < 8 \text{nm}$ [30], and $0.5R_0 < r < 1.5 R_0$, which indicated that the energy transfer from BSA to Tm-Porp occurs with high probability and, then we were subsequently able to characterize effectively the conformation of this complex.

The effect of the Tm-Porp on the BSA conformation

UV-Vis: Figure 6 shows the different absorption spectra for the BSA in the wavelength range 220-340 nm at pH 7.40 and in the control of compound protein for increasing Tm-Porp concentrations. Similar observation of the fluorescence quenching, the protein spectra showed a notable increase in optical absorption intensity as the amount of drug concentrations increases. The corresponding peaks red shift (from 277.3 to 280.5 nm) was also observed. We have attributed this difference to that the cationic drugs have penetrated through the hydrophobic pocket of the Trp residues and inevitably led to change the environment of Trp residues. This is also responsible for extending of the peptide strands of BSA and strengthening of hydrophobicity of chromophore's microenvironment, with the result having the formation ground-state complex as compared with an unbound protein. The formation of the rigidity portion of the protein with the force of electrostatic interactions preferentially engendered the mechanical strength in contrast to the native one [31]. And the absence of water in the molecular interior with coming into being of a more stiffness portion of the protein matrix may be directly altered the whole chain conformation under the influence of a drug.

Circular dichroism: For more detailed information on the conformation of the drug to BSA, CD measurements of Tm-Porp with BSA were carried out at pH 7.40 in the UV-Vis region at different R

values. The CD spectra of BSA in the absence (A) and presence (B–F) of the drug are shown in (Figure 7), where the CD spectra of protein exhibit two mainly negative bands in the UV region at 208 and 222 nm, which are characteristic of an α -helical structure of BSA. At low Tm-Porp concentration (≤ 0.10 mmol/L or $R \leq 1$), there is little change in the helicity, implying that the secondary structure of BSA is possibly stabilized by Tm-Porp. When the concentration of Tm-Porp is 0.15 mmol/L, the molar ratio(R) of Tm-Porp to BSA more than 1.0 could cause the secondary structure of BSA to be disrupted. In addition, at high Tm-Porp concentration (> 0.15 mmol/L), the percentage of α -helix content has to tend to zero fast, at the same time the β -sheet and random coil conformation are the principal component, indicating that Tm-Porp at high concentration absolutely has disrupted the secondary structure and led to the unfolding and extending of BSA.

CD spectrum is usually presented in molar ellipticity [$\theta(\lambda)$] unit ($\text{deg}\cdot\text{cm}^2\cdot\text{dmol}^{-1}$), for proteins, the mean residue ellipticity (MRE) can be calculated as follows [32]:

$$MRE = \frac{\text{ObservedCD}(m\text{ deg})}{C_p n l \times 10} \quad (8)$$

where C_p is the molar concentration of the protein, n is the number of amino acid residues and l is the path length in cm. The α -helix content of BSA estimated from MRE values at 208 nm is given by [33]:

$$\alpha\text{-Helical}(\%) = \frac{-MRE_{208} - 4,000}{33,000 - 4,000} \times 100 \quad (9)$$

Here MRE_{208} is the observed MRE value at 208 nm, 4,000 is the gross MRE of the β -sheet and random coil conformation at 208 nm, and 33,000 is the gross MRE of a pure α -helix at 208 nm.

At low Tm-Porp concentration, that is when the value of ligand/BSA ratio R was smaller or equal to 1 as shown in (Table 3), the percentage of α -helix content has decreased from 47.23% to 43.89%. According to the literature [34], the secondary structure of BSA may be stabilized by a covalent cationic crosslinking of Tm-Porp complex containing organofunctional groups, it maybe builds bridges between particular nonpolar residues and particular site-I or site-II of BSA. This results obtained are agreement with various ligands in two orientation dimensions with equal occupancy. In addition, the negative extrinsic Cotton effect (Table 3) shifts from 208.75 nm to 208.50 nm, this suggests that the drug molecules are distributed between two different binding sites with different binding properties and optical characteristics [35].

At high Tm-Porp concentration ($R > 1$), the free micelles of Tm-Porp begin to form after saturation binding of BSA with an increased Tm-Porp concentration, which leads BSA to an extended structure with exposed hydrophobic residues, implying that the electrostatic and hydrophobic interactions are the predominant intermolecular forces in stabilizing this complex.

Synchronous fluorescence spectroscopy: The third of the binding of the drug to two amino acid residues, namely the Trp and tyrosine (Tyr), was followed by estimation of the sensitivity to the surroundings district of chromophore by using SFS method. This model usually involves the fluorescence spectral simplification, spectral bandwidth reduction, non-intrusive measurement of protein in low concentration, respectively. So SFS provides a method of identifying chromophores's environment by inspecting the potential shift in wavelength and locality of maximum emission wavelength (λ_{max}) [36]. According to Miller [37], the distinction value of excitation wavelength and emission wavelength ($\Delta\lambda = \lambda_{\text{em}} - \lambda_{\text{ex}}$) denotes the spectra of disparate chromophores. With large $\Delta\lambda$ values such as 60 nm, the synchronous fluorescence of BSA is characteristic of the Trp and, small $\Delta\lambda$ such as 15

Site marker	$K_{SV} \times 10^{-5} (M^{-1})$	$K_a \times 10^{-5} (M^{-1})$
Without	1.359(0.9973) ^a	5.57(0.9944)
WF	0.75(0.9935)	3.25(0.9967)
IBP	0.77(0.9953)	3.23(0.9975)

^aThe given values in parentheses are means of the correlated coefficient

Table 3: Effects of site probe on the binding of cationic Tm-Porp to BSA (297K).

protein	R	$\lambda_{1\text{max}}$	$\lambda_{2\text{max}}$	MRE	α -helix
BSA (C _{Tm-Porp} /C _{BSA})		(nm)	(nm)	($\text{deg}\cdot\text{cm}^2\cdot\text{dmol}^{-1}$)	(%)
	0	208.75	221.85	1.77×10^4	47.23
	0.5	208.65	222.25	1.70×10^4	44.94
	1.0	208.50	222.25	1.67×10^4	43.89
	1.5	208.34	223.10	1.13×10^4	25.40
	2.0	207.94	224.00	0.37×10^4	≈ 0
	2.5	207.66	224.10	0.32×10^4	≈ 0
	3.0	207.60	224.20	0.28×10^4	≈ 0

Table 4: The Circular dichroism spectra results for Tm-Porp-BSA complexes in far-UV regions.

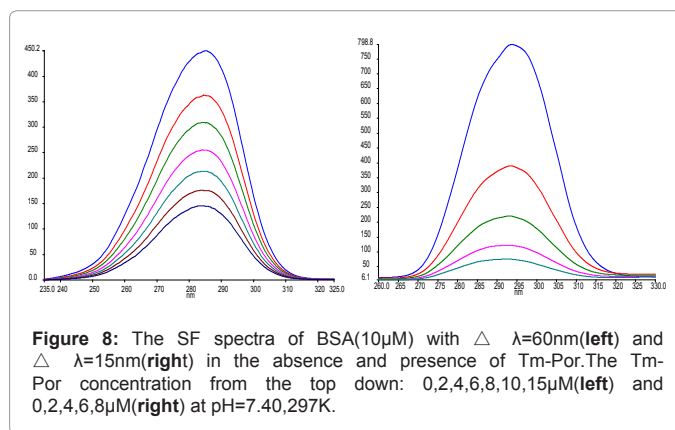


Figure 8: The SF spectra of BSA(10 μ M) with $\Delta\lambda=60\text{nm}$ (left) and $\Delta\lambda=15\text{nm}$ (right) in the absence and presence of Tm-Por. The Tm-Por concentration from the top down: 0,2,4,6,8,10,15 μ M(left) and 0,2,4,6,8 μ M(right) at pH=7.40,297K.

nm is characteristic of Tyr. The SFS of BSA with various concentrations of Tm-Porp was recorded at $\Delta\lambda=60$ nm (Figure 8. left) and $\Delta\lambda=15$ nm (Figure 8. right) respectively. With a concentration of the BSA being unvaried and the concentration of Tm-Porp increasing by titration method, we could be able to observe both very notably decreased in emission intensity due to increasing drug concentrations. The spectra of Trp showed a decrease in drug from 100% to 29% at 286 nm and with a little shift of maximum wavelength were observed. Meanwhile, the spectra of the Tyr showed a dramatically decrease from 100% to 9% at 294 nm and with a shift of the emission band edge towards the shortwave range from 294 nm to 291 nm (blue-shift) were also observed. The former phenomenon is attributed to the formation of a ground state complex between chromophore and drug. Then, the fluorescence band exhibits an inconspicuous shift at low Tm-Porp concentration ($R \leq 1$), which is due to a little change of the configuration in Trp including subdomains IIA and IIIA.

Nevertheless, the characteristics of significant approach to quenching suggest that the movement of the Trp residues was placed in a more hydrophobic environment, leading to a corresponding polarity around the Trp residues weakening and its hydrophobicity strengthening [38]. However, the latter phenomenon is ascribed to the change in conformation near Tyr's areas and with preferential rearrangement of its microenvironment. On the other hand, the λ_{max} of the Tyr shifted to shorter wavelengths via alternatively conformational changes near the Tyr as a consequence of binding, and it seems logical that the Tyr is near the binding site [24]. For the target residues are

located mainly in subdomain IIIA (Tyr 263) and IIA (Tyr140, Tyr148, Tyr150, Tyr156 and Tyr157) [25,36], (excluded the recombinant domain III, which includes residues 377–583), as we expected, it can be attributed this difference to the quencher for parallel-access to two kinds of the binding site, not only in a conformationally adaptable region site-I, but also in a clinical pharmacology of drug-specific site-II. The results obtained by SFS are in excellent agreement with experiment by using fluorescence quenching and probe competitive displacement methods. In addition, a small intra target dosage of this drug implied that the cationic Tm–Porp would be able to bind to BSA with higher affinity.

Conclusions

We have characterized the interactions between the cationic Tm–Porp and BSA by using a fluorescence quenching mechanism and a modified Scatchard equation approach as well as on the application of Förster's non-radiative energy transfer theory. We also have provided an approach for performing a structural site probe competition. The effect of Tm–Porp on conformational characteristics of BSA was a direct consequence of the mutually conjugate with respect to hydrophobic and electrostatic interactions by using UV-Vis, CD and SFS spectroscopic measurements. The corresponding thermodynamic parameters ΔH^0 , ΔG^0 and ΔS^0 indicates that the Tm–Porp quenches the fluorescence emission of BSA through a static quenching procedure. The binding parameters, such as K_{sv} , n , and r had been calculated according to the relevant theories and data. Our studies on the interaction of Tm–Porp with BSA show that the cationic Tm–Porp can bind at the site-I and site-II of BSA with equal occupancy and high affinity. Moreover, the Tm–Porp binding on site-II of BSA is expected to enable it as a potential detection reagent for tumor markers and PDT in vivo. Finally, this study can provide a richly detailed view of the interactions between protein and metalloporphyrins that can be useful for drug design and pharmaceutical research.

Acknowledgements

We are grateful to Laboratorial Chemistry Education Center of Wuhan University for their generous gifts of the chemical preparations and measuring instruments supply. We also thank Dr. Q. Xiao for energy transfer calculation technical help and Dr. Z.D. Qi for critical reading of the manuscript.

References

1. Milgram L, MacRobert S (1998) *Chem. Br* 34: 45.
2. Chatterjee S, Srivastava TS (2000) Spectral investigations of the interaction of some porphyrins with bovine serum albumin. *J Porphyrins Phthalocyanines* 4: 147–157.
3. Andrade SM, Costa SM (2002) Spectroscopic studies on the interaction of a water soluble porphyrin and two drug carrier proteins. *Biophysics J* 82: 1607–1609.
4. Silva D, Cortez CM, Louro SR (2004) Quenching of the intrinsic fluorescence of bovine serum albumin by chlorpromazine and hemin. *Braz J Med Biol Res* 37: 963–968.
5. Smetana Z, Malik Z, Orenstein A, Mendelson E, Ben-Hur E (1998) Treatment of viral infections with 5-aminolevulinic acid and light. *Lasers Surg Med* 21: 351–358.
6. Ni JZ (1995) *Bioinorganic Chemistry of Rare Earth Elements*. Science Press, Beijing p.18.
7. Bonnett R, Martinez G (2001) Photobleaching of sensitizers used in photodynamic therapy. *Tetrahedron* 57: 9513–9547.
8. Wong CP, Venteicher RF, Horrocks WD Jr (1974) Letter: Lanthanide porphyrin complexes. A potential new class of nuclear magnetic resonance dipolar probe. *J Am Chem Soc* 96: 7149–50.
9. Pandey RK, Constantine S, Tsuchida T, Zheng G, Medforth CJ, et al. (1997) Synthesis, photophysical properties, in vivo photosensitizing efficacy, and human serum albumin binding properties of some novel bacteriochlorins. *J Med Chem* 40:2770.
10. Reddi E (1997) Role of delivery vehicles for photosensitizers in the photodynamic therapy of tumours. *J Photochem Photobiol B* 37:189–195.
11. Griffiths SJ, Heelis PF, Heylett AK, Moore JV(1998) Photodynamic therapy of ovarian tumours and normal cells using 5,10,15,20-tetra-(3-carboxymethoxyphenyl)-chlorin. *Cancer Lett* 125: 177.
12. Hou AX, Xuea Z, Liu Y, Qu SS, Wong WK (2007) Antibacterial effects of a monoporphyrinato ytterbium(III) complex and its free components on *Staphylococcus aureus* as determined by stop-flow microcalorimetry. *Chemistry & Biodiversity* 4:1492–1500.
13. Bennett M, Krah A, Wien F, Garman E, McKenna R, et al. (2000) A DNA-porphyrin minor-groove complex at atomic resolution: the structural consequences of porphyrin ruffling. *Proc Natl Acad Sci USA* 97: 9476–9481.
14. Uddin SJ, Shilpi JA, Murshid GMM (2004) Determination of the binding sites of arsenic on bovine serum albumin using warfarin (site-I specific probe) and diazepam (site-II specific probe). *J Biol Sci* 4: 611–612.
15. Adler AD, Longo FR., Finarelli JD (1976) *J Org Chem* 32:476.
16. Lakowicz JR (2006) *Principles of Fluorescence Spectroscopy*, 3rd ed. Plenum Press, New York, p 55–57 and p 214, 308.
17. Kamat PV (2002) Photophysical photochemical and photocatalytic aspects of metal nanoparticles. *J Phys Chem B* 106:7729–7744.
18. Papadopoulou A, Green RJ, Franzier RA (2005) Interaction of flavonoids with bovine serum albumin: a fluorescence quenching study. *J Agric Food Chem* 53:158–163.
19. Lakowicz JR, Weber G (1973) Quenching of fluorescence by oxygen. A probe for structural fluctuations in macromolecules. *Biochemistry* 12: 4161–4170.
20. Yang MM, Xi XL, Yang P, Chin (2006) Study of the Interaction of Cephalosporin Class Medicine with Albumin by Fluorescence Enhancement and Fluorescence Quenching Theories. *J Chem* 24: 642–648.
21. Ross DP, Subramanian S (1981) Thermodynamics of protein association reactions: forces contributing to stability. *Biochemistry* 20: 3096–3102.
22. Maruyama A, Lin CC, Yamasaki K, Miyoshi T, Imai T, et al. (1993) Binding of suprofen to human serum albumin. Role of the suprofen carboxyl group. *Biochem Pharm* 45: 1017–1026.
23. Guo M, Zou JW, Yi PG (2004) Binding interaction of gatifloxacin with bovine serum albumin. *Analytical Sciences Japan* 20: 466–469.
24. Colmenarejo G (2003) *In silico* prediction of drug-binding strengths to human serum albumin. *J Med Res Rev* 23: 275.
25. Zhou N, Liang YZ, Wang P (2008) Characterization of the interaction between furosemide and bovine serum albumin. *J Molecular Structure* 872: 190–196.
26. Petiipas I, Bhattachaya AA, Twine S (2001) Crystal structure analysis of warfarin binding to human serum albumin: anatomy of drug site I. *J Biological Chem* 276: 22806–22807.
27. Stewart AJ, Blindauer CA, Berezenko S (2003) Interdomain zinc site on human albumin. *Proc Natl Acad Sci USA* 100: 3701–3706.
28. Qi ZD, Zhou B, Xiao Q, Shi C (2008) Interaction of rofecoxib with human serum albumin: Determination of binding constants and the binding site by spectroscopic methods. *J Photochem Photobiol A: Chem* 193: 81–88.
29. Cyril L, Earl JK, Sperry WM (1961) *Biochemists Handbook*, E & FN Epon Led. Press, London, p 83.
30. Schwarz G (1976) *Biophysics of Structure and Mechanism* 2: 3–11.
31. Hu YJ, Liu Y, Pi ZB, Qu SS, Bioorg (2005) Interaction of cromolyn sodium with human serum albumin: a fluorescence quenching study. *Bioorg Med Chem* 13: 6609–6614.
32. Andrew J, Milesa, Wallace BA (2006) Synchrotron radiation circular dichroism spectroscopy of proteins and applications in structural and functional genomics. *Chem Soc Rev* 35: 39–51.
33. Yuan V, Xu JG, Chen GZ (1997) *Science in China Ser B* 29: 18.
34. Li YJ, Wang XY, Wang YL (2006) *J Phys Chem B* 110: 8499.

35. RK Dockal M, Daniel C, Carter, Florian (1999) The three recombinant domains of human serum albumin. Structural characterization and ligand binding properties. *J Biological Chem* 274: 29303 –29310.
36. Sulkowska A, Rownicka J, Bojko B (2004) Effect of guanidine hydrochloride on bovine serum albumin complex with antithyroid drugs: fluorescence study. *J Mol Struct* 704: 291-295.
37. Miller JN (1979) *Proc. Anal. Div. Chem. Soc.* 16: 203-209.
38. Klajnert B, Bryszewska M (2002) Fluorescence studies on PAMAM dendrimers interactions with bovine serum albumin. *Bioelectrochemistry* 55: 33–55.